ACS APPLIED MATERIALS & INTERFACES

UCONN LIBRARIES

Subscriber access provided by UNIVERSITY OF CONNECTICUT

Article

Effect of BN Nanoparticles Loaded with Doxorubicin on Tumor Cells with Multiple Drug Resistance

Irina Zhitnyak, Igor Bychkov, Irina V. Sukhorukova, Andrey M. Kovalskii, Konstantin Firestein, Dmitri Golberg, Natalya Gloushankova, and Dmitry V. Shtansky

ACS Appl. Mater. Interfaces, **Just Accepted Manuscript** • DOI: 10.1021/acsami.7b08713 • Publication Date (Web): 31 Aug 2017

Downloaded from http://pubs.acs.org on September 1, 2017

Just Accepted

"Just Accepted" manuscripts have been peer-reviewed and accepted for publication. They are posted online prior to technical editing, formatting for publication and author proofing. The American Chemical Society provides "Just Accepted" as a free service to the research community to expedite the dissemination of scientific material as soon as possible after acceptance. "Just Accepted" manuscripts appear in full in PDF format accompanied by an HTML abstract. "Just Accepted" manuscripts have been fully peer reviewed, but should not be considered the official version of record. They are accessible to all readers and citable by the Digital Object Identifier (DOI®). "Just Accepted" is an optional service offered to authors. Therefore, the "Just Accepted" Web site may not include all articles that will be published in the journal. After a manuscript is technically edited and formatted, it will be removed from the "Just Accepted" Web site and published as an ASAP article. Note that technical editing may introduce minor changes to the manuscript text and/or graphics which could affect content, and all legal disclaimers and ethical guidelines that apply to the journal pertain. ACS cannot be held responsible for errors or consequences arising from the use of information contained in these "Just Accepted" manuscripts.

ACS Publications

ACS Applied Materials & Interfaces is published by the American Chemical Society. 1155 Sixteenth Street N.W., Washington, DC 20036

Published by American Chemical Society. Copyright © American Chemical Society. However, no copyright claim is made to original U.S. Government works, or works produced by employees of any Commonwealth realm Crown government in the course of their duties.

Effect of BN Nanoparticles Loaded with Doxorubicin on Tumor Cells with Multiple Drug Resistance

Irina Y. Zhitnyak[1], Igor N. Bychkov[1], Irina V. Sukhorukova[2], Andrey M. Kovalskii[2], Konstantin L. Firestein[2,3], Dmitri Golberg[3,4], Natalya A. Gloushankova[1], Dmitry V. Shtansky[2]

[1]*N.N. Blokhin Russian Cancer Research Center, Kashirskoe shosse 24, Moscow 115478, Russia*

[2]*National University of Science and Technology "MISIS", Leninsky prospect 4, Moscow, 119049, Russia*

[3]*School of Chemistry, Physics and Mechanical Engineering, Queensland University of Technology (QUT), 2nd George st., Brisbane, QLD 4000, Australia*

[4]*Intrenational Center for Materials Nanoarchitectonics (MANA), National Institute for Materials Science (NIMS), Namiki 1-1, Tsukuba, Ibaraki 3050044, Japan*

Keywords: DOX-BNNP nanoconjugates, drug loading, multidrug resistant tumor cells, carcinoma and leukemia cell lines, cytotoxic effect.

Research highlights

- Produced BN nanoparticles revealed numerous nanosheet-like petals
- High efficiency of BN nanoparticle saturation with doxorubicin was documented
- DOX-BNNPs were well internalized by MDR cells and distributed in cytoplasm near nucleus
- Higher sensitivity of leukemia lines to DOX-BNNPs was evidenced compared with carcinoma lines
- Utilization of DOX-BNNPs allowed to maintain high and stable level of DOX in MDR cells

Abstract

Herein we study the effect of doxorubicin-loaded BN nanoparticles (DOX-BNNPs) on cell lines that differ in the multidrug resistance (MDR), namely KB-3-1 and MDR KB-8-5 cervical carcinoma lines, and K562 and MDR i-S9 leukemia lines. We aim at revealing the possible differences in the cytotoxic effect of free DOX and DOX-BNNP nanoconjugates on these types of cells. The spectrophotometric measurements have demonstrated that the maximum amount of DOX in the DOX-BNNPs is obtained after saturation in alkaline solution (pH 8.4), indicating the high efficiency of BNNPs saturation with DOX. DOX release from DOX-BNNPs is a pH-dependent and DOX is more effectively released in acid medium (pH 4.5–5.5). Confocal laser scanning microscopy has shown that the DOX-BNNPs are internalized by neoplastic cells using endocytic pathway and distributed in cell cytoplasm near the nucleus. The cytotoxic studies have demonstrated a higher sensitivity of the leukemia lines to DOX-BNNPs compared with the carcinoma lines: IC_{50}(DOX-BNNPs) is 1.13, 4.68, 0.025, and 0.14 μg/ml for the KB-3-1, MDR KB-8-5, K562, and MDR i-S9 cell lines, respectively. To uncover the mechanism of cytotoxic effect of nanocarriers on MDR cells, DOX distribution in both the nucleus and cytoplasm has been studied. The results indicate that the DOX-BNNP nanoconjugates significantly change the dynamics of DOX accumulation in the nuclei of both KB-3-1 and KB-8-5 cells. Unlike free DOX, the utilization of DOX-BNNPs nanoconjugates allows for maintaining a high and stable level of DOX in the nucleus of MDR KB-8-5 cells.

1. INTRODUCTION

Various nanomaterials (with dimensions of 10^{-8}-10^{-9} m) are widely used in contemporary medicine. The first micellar drug Sandimmune® was clinically approved in 1983, and the first drug-polymer nanoconjugate Adagen® began to be used in medicine in 1990.[1] Since then, the increased interest in diagnostic and therapeutic nanotools has led to the appearance of a number of biomedical nanotechnologies, including nanoconjugates of pharmaceutical drugs with proteins,[2] micelles,[3] liposomes,[4] dendrimers,[5] inorganic nanoparticles[6, 7-11] etc. More than two dozens nanotechnologies have been approved for diagnostic and therapeutic use in the clinics, and many others are at the clinical research stage.

The use of chemotherapeutic drugs for the treatment of cancer is restrained by the appearance of so-called multidrug resistant (MDR) tumor cells during the evolution of the malignant phenotype. There are several known mechanisms of MDR, which are essentially adaptations to cellular stress: increased drug efflux, decreased drug influx, DNA repair activation, detoxification, and blockage of apoptosis.[12] The principal mechanism that confers a broad-spectrum drug resistance on the MDR cells is increased drug efflux from the malignant cells by multidrug membrane transporters (e.g., P-glycoprotein, Pgp).[13] The problem of MDR overcoming can be resolved with the use of nanotransporters which facilitate drug entry into the cell through caveolin-mediated endocytosis. It is important to safely deliver the drug to the site of injury without drug leakage. Low solubility in an aqueous solution, short half-life, and high toxicity to normal tissue may hinder the efficiency of nanoconjugated anticancer drugs, as well as free drugs. In contrast, nanoparticles can be accumulated in tumors by extravasation from tumor blood vessels that exhibit enhanced vascular permeability (the phenomena of enhanced permeability and retention (EPR)). Nanoparticle drug delivery systems may improve the therapeutic index of the loaded chemotherapeutic drugs compared to free drugs; increase drug efficacy by achieving steady state therapeutic levels of drugs over an extended period; and lower drug toxicity due to controlled drug release and improve drug's pharmacokinetics by increasing their solubility and stability.[16] To increase selectivity of cancer therapy and decrease toxicity towards normal tissue, nanoconjugates can be functionalized with tumor-specific ligands (e.g., folic acid, HER2 antibody, and transferrin).[17-21,] Different types of nanocarriers, such as metals, polymers, lipids, carbon- and oxide-based nanoparticles, dendrimers, liposomes, micelles, et al. were developed as prospective platforms for drug delivery.[22,23]

Doxorubicin (DOX) is one of the most effective antitumor drugs. The main mechanisms by which DOX acts in the cancer cell are: (i) intercalation into DNA and binding to DNA-associated enzymes resulted in inhibition of DNA repair, ceasing DNA replication and RNA

transcription, and (ii) generation of free radicals that cause DNA and protein damage.[24] Note, however, that the usage of DOX in cancer therapy is limited because of its strong cardiotoxicity at high concentrations, the accumulation effect in organs, and selection of drug-resistant tumor cells.[14] DOX-loaded liposomes (Doxil) were the first FDA-approved nanodrug successfully utilized in clinical practice.[25] Despite their high therapeutic efficiency, a number of serious problems remain unresolved: Doxil may severely reduce the number of blood cells that may potentially increase the risk of infections, anemia, and bleeding; occurrence of heart-related side effects, hand-foot syndrome, oral cancer after prolonged therapy, temporary or permanent infertility, and peripheral neuropathy.[26-28] Recent developments in advanced mesoporous silica nanoparticles for drug delivery represent promising avenues for the management of MDR associated with cancer therapy, but their therapeutic effectiveness remains low.[29]

In recent years there has been increased attention to more sophisticated nanostructures, such as quantum dots, nanosheets, and nanotubes. Carbon nanotubes (CNTs) are the most widely used hybrid inorganic nanomaterial. They are promising candidates for medical applications but conflicting data on their toxicity limits their wide clinical use.[30] Boron nitride (BN) nanotubes are structural analogues of carbon nanotubes. Their mechanical properties match those of CNTs, while their increased chemical and thermal stability gives them a competitive advantage in development and production of new types of biomaterials.[31-34] Previous research[35] has demonstrated a pronounced cytotoxic action of chemotherapeutic molecules conjugated with BN nanostructures in tumor cell cultures. Specifically, use of BN nanotubes (modified with mesoporous silica) increased efficiency of intracellular delivery of doxorubicin 3-4 fold.

BN-based nanoparticles (BNNPs) are of great interest as catalytic supports, reinforcing agents, and drug-loaded nanocarriers. Our previous study has demonstrated that the BNNPs loaded with doxorubicin (DOX-BNNPs) are stable at neutral pH but effectively release DOX at pH 4.5−5.5. MTT assay and cell growth tests have shown that DOX-BNNPs is toxic for neoplastic IAR-6-1 cells. The DOX-BNNPs nanocarriers have been internalized into IAR-6-1 neoplastic cells using endocytic pathways, and then DOX has been released from nanosized drug delivery carriers and accumulated in both nuclei and cytoplasm, resulting in cell death.[36] Recently, an exciting new therapeutic effect of hollow BN spheres with controlled release of boron for prostate cancer treatment has been demonstrated. Hollow BN spheres induce apoptosis and inhibit the proliferation for both the androgen-sensitive LNCap and androgen-independent DU145 prostate cancer cells. In vivo assay has demonstrated that hollow BN spheres significantly suppress the tumor occurrence and growth in male BALB/c-nu/nu mice models injected with LNCap prostate cancer cells.[37]

Herein we study the effect of DOX-BNNP nanoconjugates on cell lines that differ in the multidrug resistance, namely two lines of cervical carcinoma and two lines of leukemia. We are aiming at revealing the possible differences in the cytotoxic effect of free DOX and DOX-BNNPs on these types of cells. To uncover the mechanism of cytotoxic effect of nanoconjugates on MDR cells, DOX distribution in both the nucleus and cytoplasm of different cell lines has thoroughly been studied.

2. MATERIALS AND METHODS

2.1. Synthesis of BNNPs. Nanoparticles were synthesized in a boron oxide CVD process in a vertical induction heating reactor, as described elsewhere.[38] Compared with the previous syntheses, the composition of precursor and the temperature in precursor zone were changed to reduce the oxidation state and increase the purity of BNNPs. The powder mixture of $BLiO_2$ (99.9%), MgO (analytical grade), and pure *h*-BN taken in a molar ratio 2:1.2:2 was used as a precursor. Magnesia was calcined in air at 450°C for 1 h for dehydration just before weighing. Precursor mixture was mechanically ground in an alumina mortar for 1 h. Argon of 99.993% purity was used as a carrying gas, supplied at a feeding rate 300 cm^3/min from the bottom of the reactor, and ammonia of 99.98% purity was used as the reactant gas, supplied at a feeding rate 75 cm^3/min from the top. The furnace chamber was evacuated to a pressure of 10^{-2} mbar under slow heating to 360 ^oC. Then, an argon flow was introduced, the pressure of 1 bar was maintained, and heating to the synthesis temperature was started. Synthesis was carried out under the temperature gradient along the reactor height between 1400°C in the precursor zone (at the bottom of the reactor) and 750°C in the BN particles outlet zone (at the top of the reactor) for 4 h. The temperature of the powder mixture was controlled by an optical pyrometer during the whole experiment.

2.2 Characterization of BNNPs. The morphology and chemical composition of synthesized products were studied using a scanning electron microscope JSM-7600F (JEOL) equipped with the EDX detector. Particle size distribution was estimated using dynamic light scattering method on a particle size analyzer (Zetasizer Nano ZS). Transmission electron microscopy (TEM) studies, including high resolution TEM (HRTEM) and high-angular dark field scanning TEM (HADF-STEM) imaging, were carried out using a JEM 2100 microscope (JEOL) operated at 200 kV. The chemical compositions of as-synthesized BNNPs and those after saturation with DOX were analyzed by Fourier-transform infrared spectroscopy (FTIR) using a Vertex 70v vacuum spectrometer (Bruker) in the range of 400–2000 cm^{-1} with the partial internal reflection device and Raman spectroscopy using a NT-MDT NTEGRA Spectra instrument with an excitation wavelength of 473 nm.

2.3. Saturation of BNNPs with DOX, Preparation of DOX-BNNPs. For study of efficiency of DOX loading into BNNPs at various pH, 2 mg of BNNPs were added to 0.5 ml of DOX (Teva) solutions (0.5 mg/ml in 0.1 M sodium acetate buffer) at different pH values of 5.4, 7.4, 8.4, and 9.4. The suspensions were incubated at 37°C for 24 h with shaking. Then the BNNPs were washed out from DOX in water 5 times under repeated centrifugation at 13400 rpm for 15 min. For cytotoxic experiments, saturation of 2 mg of BNNPs with DOX was performed in 1 ml of 0.5 mg/ml DOX solution in 0.1 M sodium acetate buffer, pH 8.4.

2.4. Drug Loading Capacity. The amount of DOX loaded into BNNPs was determined by comparing the intensities of the absorption of DOX in the initial DOX solution used for loading of BNNPs with the supernatant DOX solution after removal of all DOX-BNNPs. 0.2 ml of samples were analyzed by a "Benchmark Plus" spectrophotometer (Bio-Rad) at the laser wavelength of 488 nm using "Microplate Manager 5.2.1" software .

2.5. Drug Release. For the drug release study, 1 mg of DOX-BNNPs was suspended either in 1 ml of phosphate buffer saline (PBS) or 0.1 M sodium acetate buffer (NaAc) at different pH values (pH 4.0, 5.0, 6.0, and 7.4) for 24 h. Supernatants (0.2 ml) were analyzed by means of "Benchmark Plus" spectrophotometer at laser wavelength of 488 nm.

2.6. Cell Culture. The parent KB-3-1 cell line was established from a single clone of KB human cervical carcinoma cell line.[39,40] The multidrug-resistant KB-8-5 subline was derived from KB-3-1 line by a series of step selections in colchicine.[39] The cells were cultured in Dulbecco's modified Eagle's medium (DMEM) from Sigma supplemented with 10% fetal bovine serum (FBS) from PAA Laboratories, penicillin (100 IU/ml), and streptomycin (100 μg/ml) at 37°C in a 5% CO_2-humidified atmosphere. Before cell culture tests, the KB-8-5 cells were cultured in a DOX environment (100 ng/ml) for 2 weeks and then for 3 weeks without DOX.

We also used the myelogenous leukemia K562 cell line and the multidrug-resistant i-S9 subline established from K562 culture after stable transfection with P-glycoprotein.[41] The cells were cultured in RPMI medium (Gibco) supplemented with 10% FBS, penicillin (100 IU/ml), and streptomycin (100 μg/ml) at 37°C in a 5% CO_2-humidified atmosphere. Before the experiments began, i-S9 cells were cultured in a DOX environment (100 ng/ml) for 2 weeks and then for 3 weeks without DOX.

2.7. Internalization of BNNPs by Cells and Fluorescence Imaging. The KB-3-1 and KB-8-5 cells (50 000 cells/ml in 2 ml of medium) were seeded into 35 mm glass-bottom culture dishes (MatTek Corporation) and incubated for 24 h. Free DOX (4.25 μg/ml), DOX-BNNPs (34 μg/ml), and BNNPs (34 μg/ml) were added to the culture medium. After 24 h of incubation, cells were fixed with 3.7% paraformaldehyde (PFA) at room temperature for 10 min, then

permeabilized with 0.5% Triton X-100 for 3 min, and finally stained with Alexa488-phalloidin for 40 min. For the visualization of nanoparticles and main cytoplasmic structure, actin cytoskeleton, a confocal laser scanning microscope (CLSM) (Leica TCS SP5) was used.

For staining with LysoTracker cells were seeded into 35 mm glass-bottom culture dishes. After 24 h incubation, 34 μg/ml of DOX-BNNP suspension was added to the culture medium for 8 h. For live-cell imaging, cells were transferred into phenol red-free DMEM/F-12 medium with HEPES (Sigma) supplemented with 10% FBS and incubated with LysoTracker Green DND-26 (Invitrogen) (50 nM) at 37 °C for 30 min. The cells were examined in green, red and differential interference contrast (DIC) channels of CLSM.

2.8. Cell Counting. Cells were seeded into 24-well plates with coverslips (1.9 ml of medium per well, $2x10^4$ cells/ml) and incubated for 24 h. The prescribed amounts of BNNPs, DOX-BNNPs, and free DOX at different concentrations were added to the cell cultures. After 72 h incubation, cells were fixed with 3.7% PFA at room temperature for 10 min. The fixed specimens were incubated for 40 min with 4',6-diamidino-2-phenylindole (DAPI) and then examined with a "Zeiss Axioplan" microscope equipped with a Plan Fluor 40x objective. Stained with DAPI nuclei were counted in 20 objective fields using ImageJ 1.51n (Fiji) Software and Cell Counter plugin. Cell viability was expressed as a percentage of treated cells to the number of untreated control cells.

2.9. Flow Cytometry. K562 and i-S9 cells were plated in 96-well plates (200 μl per well, $2x10^4$ cells/ml) in RPMI medium supplemented with 10% FBS and a mixture of penicillin (100 IU/ml) and streptomycin (100 μg/ml). After 24 h, the prescribed amounts of BNNPs, DOX-BNNPs, and free DOX at different concentrations were added and incubated in an 5% CO_2 atmosphere at 37°C for 72 h. Before cell density measurements, the K562 and i-S9 cells were treated with propidium iodide for dead cells detection. Using a flow BD FACSCanto TM II cytometer (BD Biosciences) equipped with BD FACSDiva software, the number of living cells in 200 μl of sample volume was measured. The time of measurement was 80 s. Cell viability was expressed as a percentage of treated cells to the number of untreated control cells.

2.10. MTT Assay. The cells were plated in 96-well plates (200 μl per well, 2 x 10^4 cells/ml) using DMEM supplemented with 10% FBS and a mixture penicillin (100 IU/ml) and streptomycin (100 μg/ml). After 24 h, the prescribed amounts of free DOX at different concentrations were added and cells were incubated in an 5% CO_2 atmosphere at 37°C for 72 h. Then the medium was aspirated and replaced by fresh FBS-free medium and 3-(4,5-dimethylthiazol-2-yl)-2,5-diphenyl-2*H*-tetrazolium bromide (MTT) solution in PBS (20 μl, 5 mg/ml) was added. After incubation for 4 h, the supernatant was carefully aspirated, and the MTT-formazan generated by live cells was dissolved in 150 μl of DMSO for 20 min. The

absorbance at a wavelength of 570 nm was measured by means of a microplate "Benchmark Plus" spectrophotometer (Bio-Rad). Non-treated cells were utilized as control. The absorbance was normalized to the blank (150 µl DMSO) and expressed as a percentage of viable cells.

2.11. Fluorescence Intensity Measurements. 160 000 cells/ml were seeded into 35 mm culture dishes in 2 ml of medium and incubated for 24 h. DOX water solution and DOX-BNNP suspension were added to 24 h culture cells at the appropriate IC_{50} concentrations obtained from cell counting assay. For KB-8-5 cells, additional samples with IC_{50} determined for KB-3-1 were used as controls. After 2, 8, 24, and 48 h of incubation with either DOX or DOX-BNNPs, cells were fixed with 3.7% PFA at room temperature for 10 min. Then the samples were examined with a "Nikon Eclipse Ti-E" microscope (Nikon) for imaging 10 fields for each sample in DIC and fluorescent channels. The fluorescence intensity (FI) was estimated using "ImageJA 1.45b" (Fiji) software by measuring mean gray value (MGV) parameter for background area (BG), cytoplasm (CP), and nucleus (N) for two cells per frame. The fluorescence intensity was calculated by the formula:

$$FI_{N/CP} = (MGV_{N/CP} - MGV_{BG}) / MGV_{BG}.$$

3. RESULTS

3.1 Characterization of BNNPs. TEM images of a BNNP and its nanosheet-like petals are shown in Fig. 1a-d. The BNNPs are formed by numerous curved BN nanosheets, 10-40 nm in length and 5-10 nm in width, with a characteristic interplanar spacing of 0.33 nm (Fig. 1d). Particle size analysis of BNNPs performed after ultrasonic treatment revealed that a major fraction of nanoparticles falls within the range of 110 – 300 nm, with most of the BNNPs (35%) having size of about 135 nm (Fig. 1e). The Raman spectrum of the as-fabricated BNNPs presented in Fig. 1f is characterized by the presence of a characteristic peak at 1369 cm^{-1} that corresponds to in-plane vibrations between B and N atoms. Figure 1g compares the FTIR spectra of BNNPs, free DOX, and DOX-BNNPs samples. The BNNPs show two characteristic features in their FTIR spectrum: a sharp low wavenumber mode at 769 cm^{-1} and a broad maximum with high intensity at 1359 cm^{-1}, which correspond to out-of-plane B-N-B bending and in-plane B-N stretching vibrations, respectively. The doxorubicin spectrum is characterized by a number of peaks that can be ascribed to NH_2 or OH (3300 cm^{-1}), C-H (2883 cm^{-1} and 1200-1400 cm^{-1}), C-O stretching (1000-1200 cm^{-1}), and out-of-plane O-H bending (700-900 cm^{-1}).[42-44] After saturation of BNNPs with DOX, some of these peaks are well distinguishable in the FTIR spectrum of DOX-BNNPs sample, hereby indicating the presence of drug on the nanoparticle surface.

Figure 2 presents TEM and HADF-STEM images, as well as corresponding EDX mapping of BN nanoparticles saturated with DOX and carboplatin (CP). The BNNPs loaded with CP were used as a model system to better visualize the drug inside the BNNPs using platinum as a marker. It can be seen that the BNNPs are in a DOX shell, 15-25 nm thick (Fig. 2a-c). Since carbon is the main component of DOX, EDX mapping indicates the uniform DOX distribution over the BNNP surface. In case of CP, the TEM image did not reveal a continuous drug layer on the BNNP surface, whereas the EDX mapping clearly demonstrates the homogeneous saturation of the BNNPs with CP (Fig. 2d-f).

3.2. DOX Loading Efficiency of BNNPs. First, we studied the efficiency of DOX loading into BNNPs in DOX solutions with different pH values (Fig. 3a). The spectrophotometric analysis of DOX solutions after BNNP saturation showed that the concentration of free DOX had dramatically decreased with increasing pH of solution, indicating more effective DOX loading at a higher pH (8.4-9.4). In DOX-BNNPs, the DOX content after saturation of 2 mg/ml of BNNPs in 1 ml of DOX solution (0.5 mg/ml) with pH 8.4 was 180-200 μg/mg. The spectrophotometric measurements of DOX after extraction from nanoparticles in DMSO for 24 h also suggested that the maximum amounts of DOX (85-165 μg/mg) were extracted from DOX-BNNPs loading with DOX in an alkaline solutions.

3.3 pH-Dependent Drug Release. To study a pH-sensitive drug release from DOX-BNNPs nanoconjugates were incubated in either PBS or acetate buffers at different pH for 24 h then the spectrophotometric measurements of DOX concentrations in the supernatants were performed. As shown in Fig. 3b, incubation of DOX-BNNPs in both PBS and acetate buffer at pH 4.4 and pH 5.4 resulted in more effective release of DOX from nanocarriers. Under these conditions, 15-20% of DOX was released from DOX-BNNPs within 24 h. Incubation of DOX-BNNPs in PBS at pH 7.4 did not lead to significant release of DOX. These data demonstrate that DOX release from DOX-BNNPs is a pH-dependent and DOX is more effectively released at acidic medium (pH 4.5–5.5) under conditions comparable to those natural for cellular endosomes/lysosomes.

3.4. Internalization of DOX-BNNPs by Cells with Different MDR Ability. Cellular uptake of free DOX, BNNPs, and DOX-BNNPs by KB-3-1 and MDR KB-8-5 neoplastic cells was studied using confocal laser scanning microscopy (Fig. 4). After 24 h of incubation, treated cells were fixed and stained with Alexa488-phaloidin to visualize the main cytoplasmic system, actin cytoskeleton. As revealed at XYZ and XZY confocal slices, DOX-BNNPs were internalized by neoplastic cells of both types and distributed in cell cytoplasm near the nucleus between actin bundles. In a red channel, it is clearly visible that both free DOX and DOX released from DOX-BNNPs were accumulated in the cell nuclei (Fig. 4f,j,p,t). Note that red

fluorescence of DOX in the nuclei of KB-3-1 cells was more intensive compared with MDR KB-8-5 cells (see Fig. 4 f and p).

To confirm the endosomal-mediated entry of DOX-BNNPs into cells LysoTracker Green, capable of labeling of highly acidic compartments within live cells, was used. Using CLSM, we examined whether DOX-BNNPs can pass through endosomal/lysosomal compartments. As shown in Figure 4u-y, in neoplastic cells, DOX-BNNPs co-localized with LysoTracker near the nucleus, hereby indicating that endocytosis is the main transport mechanism of DOX-BNNPs within cells.

3.5. Cytotoxicity of DOX-BNNPs Compared to Free DOX. The MTT assay is a commonly used colorimetric assay for assessing cell metabolic activity, which, however, does not always provide correct results in case of nanomaterials;[45-46] therefore additional independent tests are needed. Comparative studies of the cytotoxic effect of free DOX were conducted using cell viability tests: cell counting assay of DAPI stained cells and flow cytometric analysis (Fig. 5a,c) after 72 h incubation with DOX. For each line, DOX concentration, at which the cell viability decreased by half (IC_{50}(DOX)), was determined. Our results clearly demonstrated the differences in sensitivity to DOX between KB-3-1 and MDR KB-8-5 carcinoma cell lines. When we examined the number of DAPI stained cells in the field after incubation of culture with free DOX for 72 h, IC_{50}(DOX) for the KB-3-1 cells was 0.011 μg/ml, whereas for the MDR KB-8-5 cells IC_{50}(DOX) was 0.061 μg/ml. MTT test, however, showed that IC_{50}(DOX) for the KB-3-1 cells was 0.1 μg/ml and for the MDR KB-8-5 cells IC_{50}(DOX) was 2.35 μg/ml (Fig. 5e). The results implied that the cell counting of DAPI stained cells appeared to be more correct and represented the more accurate method than the MTT test; the latter measures the metabolic activity of the cells *via* tetrazolium salts. Metabolic assays may not accurately represent changes in cell growth under DOX compared to a quantitative method relying on cell counting assay. In addition, nanomaterials, for example carbon and boron nitride nanotubes, can interact with tetrazolium salts, hereby wrongly indicating nanomaterial toxicity, whereas other methods reveal no toxicity.[45,46]

We also studied the cytotoxic effect of free DOX in K562 and MDR i-S9 cultures of leukemic cells. Flow cytometric analysis of a number of living cells after 72 h incubation with DOX showed that for the K562 cell line IC_{50}(DOX) was 0.006 μg/ml, and for the i-S9 cell line IC_{50}(DOX) was 0.14 μg/ml. Note that the study of cell viability using cell counting test and flow cytometric analysis showed similar results (Fig. 5f).

Cell viability after 72 h incubation of KB-3-1, KB-8-5, K562, and i-S9 cells with either DOX-BNNPs containing 198 μg/ml of DOX or pristine BNNPs is shown in Fig 5b. For the KB-3-1 cell line IC_{50}(DOX-BNNPs) was 1.13 μg/ml, whereas for the multidrug-resistant KB-8-5 cell

line IC_{50}(DOX-BNNPs) was 4.68 μg/ml. Analysis of the viability of K562 and i-S9 cells demonstrated their higher sensitivity to DOX-BNNPs compared to the KB-3-1 and KB-8-5 carcinoma lines (Fig. 5d). The cytotoxic studies of DOX-BNNPs revealed that IC_{50}(DOX-BNNPs) was 0.025 μg/ml for the K562 cell line (approximately 40 times lower than for the drug-sensitive KB-3-1 carcinoma cell line) and 0.14 μg/ml for the i-S9 cell line (approximately 30 times lower than for the MDR KB-8-5 carcinoma cell line). In case of pristine BNNPs, cell viability tests showed that the IC_{50}(BNNPs) for KB carcinoma cell lines was greater than 470 μg/ml (Fig. 5b) For the K562 cell line IC_{50}(BNNPs) was 4.5 μg/ml and for i-S9 cell lines IC_{50}(BNNPs) was 7.5 μg/ml (Fig. 5d). These data indicate that the BNNPs exhibit low cytotoxicity in comparison with the DOX-BNNPs.

The results of cytotoxic tests of DOX-BNNPs are presented in Fig. 5b,d and the IC_{50}(DOX) and IC_{50}(DOX-BNNPs) values for different cell lines are summarized in Table 1. The spectrophotometric measurements showed that the amount of DOX in the DOX-BNNPs used in the present study was 200 μg/mg. When discussing the DOX doze in DOX-BNNPs, required to achieve IC_{50}, we should highlight that during 24 h only part of loaded DOX (15-20%) was released from DOX-BNNPs in acid medium, i.e. under conditions comparable to those existing in cellular endosomes/lysosomes (Fig. 3b). Note, however, that how many particles were internalized by cell and how much DOX was released from endocomal DOX-BNNPs into cytoplasm is not yet clear and need additional studies.

3.6. Accumulation of DOX in Both the Nucleus and Cytoplasm of Cells Differing in MDR. To distinguish differences in the impact of pure DOX and DOX-BNNP nanoconjugates on carcinoma cells differing in MDR, the dynamics of DOX accumulation in their nucleus and cytoplasm was comparatively studied. After incubation with either DOX or DOX-BNNP solutions, the fluorescence intensity of DOX was measured during 48 h in different parts of cells (Fig. 6). All cells were treated with DOX concentrations equal to IC_{50}. As a control, for KB-8-5 cells we also used IC_{50} DOX determined for KB-3-1 cell lines.

First we compared the dynamics of intensity variation in nuclei of KB-3-1 and KB-8-5 cells treated with the same free DOX dose (KB-3-1_{nucl} and KB-8-5_{nucl} (control) (Fig. 6a). In case of the KB-3-1 cells, the DOX concentration in nuclei increased over 8 h and then was maintained at approximately the same level for 48 h. In the MDR KB-8-5 cells, fluorescence intensity increased for 2 h, and then decreased, which was caused by the MDR efflux mechanism. When using a larger dose of IC_{50} (KB-8-5_{nucl} in Fig. 6a), the DOX more intensively accumulated in nuclei for 8 h. After 24 h, the DOX concentration was observed to significantly decrease due to the action of drug efflux pumps and remained relatively constant upon further exposure.

The DOX-BNNP nanoconjugates significantly changed the dynamics of DOX accumulation in the nuclei of both KB-3-1 and KB-8-5 cells. In case of the KB-3-1 cells, the DOX concentration in nuclei was observed to increase rapidly in the first 2 h and then more slowly in the next 46 h (Fig. 6b, KB-3-1_{nucl}). Most importantly, when MDR KB 8-5 cells were treated by DOX-BNNPs, after reaching the maximum DOX concentration in the cell nuclei during 8 h, the fluorescence intensity remained at the same level up to 24 h and only slightly decreased by 10% (KB-8-5_{nucl}) and 20% (KB-8-5_{nucl} (control)) in the next 24 h. Thus our results clearly indicated that, unlike free DOX, the utilization of DOX-BNNP nanoconjugates allows us to maintain a high and stable level of DOX in the nucleus of the MDR KB-8-5 cells. Note that the higher concentration of DOX released from DOX-BNNPs (Table 1) can lead to the suppression on MDR efflux mechanism.

4. DISCUSSION

When free DOX affects the KB-3-1 cells, chemotherapeutic drug penetrates through the cell membrane into the neoplastic cell cytoplasm and nucleus via diffusion and then binds with DNA. DOX to DNA interaction leads to a decrease in DOX concentration in the nucleus and promotes further diffusive penetration and accumulation of DOX in the nucleus (Fig. 6c). The DOX concentration inside the nucleus reaches saturation and eventually stops to increase when the DOX concentration inside and outside of the cell is nearly equal. When the MDR KB-8-5 cells were exposed to free DOX, diffusive penetration of the drug into the cytoplasm and nucleus activates the MDR mechanisms and the drug begins to be pumped out of the nucleus into the cytoplasm and further out of the cell (Fig. 6c). Note that the DOX diffusion into the cell continues, i.e. there is a circulation of the drug between the cell and the medium, while the accumulation of DOX in the nucleus becomes slower. Thus, in KB-8-5 cells, in order to achieve 50% of the cell death level, the DOX concentration should be increased 5.5 times compared with the KB-3-1 cells.

In discussing the results further we should first highlight that in case of nanoconjugates, the mechanism of entry of DOX-BNNPs into the cells is different from that of free DOX. The DOX-BNNPs penetrated into the KB-3-1 and KB-8-5 cells using endocytic pathway, and then DOX released in lysosomes under acid pH and diffused into the near-nuclear region of the cytoplasm and the nucleus.[36] Thus, the number of absorbed nanoconjugates determines the local DOX concentration in the cell. In sensitive KB-3-1 cells treated by DOX-BNNPs, the drug was observed to gradually accumulate in the nuclei during the whole test lasting 48 h. This observation can be explained assuming that cells continually absorb nanoconjugates, thereby ensuring a constant DOX influx into the near-nuclei zone of cells. This leads to a high

concentration zone, from which DOX further diffuses into the nucleus in which the DOX concentration is lower compared with the local concentration in the near-nuclei zone (Fig. 6c).

When the drug is delivered into the MDR KB-8-5 cells by nanoconjugates, their uptake also leads to an increase in local DOX concentration in the near-nuclear zone and further DOX influx into the nucleus. Note, however, that protective MDR mechanisms are activated which pump out the DOX back to the near-nuclei zone of the cytoplasm. Thus, in case of drug resistant cells, the continuous DOX circulation occurs, but mainly between the nucleus and cytoplasm in the perinuclear zone and there is no significant efflux of the drug into the medium. The results indicate that in the MDR KB-8-5 cells treated with DOX-BNNPs there is a compensation of the drug efflux from the nucleus through the diffusion of DOX that has been released from the absorbed nanoconjugates in the near-nuclei zone, thereby ensuring a constant concentration of DOX in the nucleus.

High nanoconjugate uptake by tumor cells and effective intracellular drug release are necessary to achieve an enhanced therapeutic effect in clinic trials. For example, the uptake rate of DOX from polyethylene glycol-modified arachidyl chitosan-based nanoparticles by K562 leukemia cells was higher compared with free DOX.[47] In vivo studies also demonstrated prolonged blood circulation of nanoparticles and sustained drug release. It was repeatedly reported that both the optimal shape and size of nanocarriers are needed to increase the uptake of drug delivery vehicles by tumor cells.[48,49] Our study demonstrated a higher sensitivity of the leukemia lines to DOX-BNNPs compared with the carcinoma lines. In discussing the therapeutic efficacy of DOX-BNNPs, it is worth noting that the spherical nanoconjugates showed rapid cellular uptake and enhanced therapeutic efficacies against MDR i-S9 leukemia cells. This is a promising result for further development of drug-loaded nanocarriers based on BN for the treatment of leukemia, including those with MDR. The DOX-BNNPs showed the ability to use endocytosis to bypass drug efflux pumps and to maintain stably high concentration of DOX in tumor cells that can enhance their therapeutic efficacy against leukemia.

Unfortunately, we can not unambiguously determine how much DOX was released within a specific cell type. Nevertheless, it is possible to make rough estimates based on the DOX loading capacity and the maximum amount of drug release, assuming that similar amount of DOX was released inside cells. According to spectrophotometric measurements of DOX concentrations, the amount of DOX in the BNNPs was 180-200 μg/mg. The spectrophotometric measurements of DOX concentrations in supernatants after DOX extraction from DOX-BNNPs in the physiological solution at acidic pH (pH 4.5−5.5) under conditions comparable to those in endosomes/lysosomes showed that approximately 15-20% DOX was released from BN nanocarriers for 24 h. Our calculations indicate that according to cell counting test, it required

1.2-7.5 (K562 cells) and 5.0-35 (IS9 cells) times less DOX conjugated with BNNPs to achieve IC_{50} compared with free DOX depending on how to estimate the effective dose of DOX in DOX-BNNPs (by loading DOX dose or by DOX release within 24 h (Table 1)). This promising result is indicative of even higher tumor cell killing ability of the DOX-BNNPs in comparison with some other conjugates. For example, IC_{50} was reduced with DOX-loaded polyisohexylcyanoacrylate nanoparticles *versus* free DOX for Huh7 (1.7 times), HepaRG (4.5 times), HepG2 (1.5 times), and HepG2.2.15 (1.5 times).[50] The IC_{50} values of DOX-loaded quantum dots-conjugated immunoliposome-based nanoparticles were reported to either decrease 2.9-fold against HER2-overexpressing SK-BR-3 cells or increased 2.8-fold against HER2 negative MCF-7 cancer cells, as compared with free DOX.[51] Antibody P-gp functionalized singlewalled CNTs loaded with DOX displayed 2.4-fold higher cytotoxicity toward MDR K562R leukemia cells than their DOX-free counterpart.[30] Note, that there are systems, for example SiO_2-siRNA-DOX conjugates, in which the antitumor effect against resistant A2780/AD human ovarian cancer cells was much higher compared with DOX-BNNPs nanocarriers,[52] but the usage of siRNA is still questionable in terms of gene toxicity.[53,54] Finally note, that further increase in the efficiency of DOX-loaded nanoconjugates can be achieved by adding a second type of antitumor drug. For example, hybrid polymer nanoparticles loaded with a mixture of DOX and Elacridar[55] showed a much higher toxicity on resistant MB435/LCC6/MDR1 cells than polymer nanoparticles saturated only with DOX on resistant MCF-7/ADR cells;[56] both nanosystems also demonstrating higher tumor cell killing ability compared with free DOX.

For the sake of completeness, recent in vivo toxicological studies of BN nanostructures should be mentioned. For example, no negative effects on blood parameters, as well as liver and kidney, were observed at different time intervals after intravenous injection of high doses of BN nanotubes.[57,58] The surface of BN nanostructures can be additionally functionalized by targeting agents to improve their biological performance. It has recently been demonstrated that cellular uptake of folate and DOX conjugated BNNTs is much higher when compared with DOX-BNNTs for HeLa cells.[59] Thus, the present and previous data indicate that, to date, a critical mass of knowledge has been accumulated, evidencing the high potential of BN nanoparticles in the biomedical field.

5. CONCLUSIONS

Doxorubicin-loaded BN nanoparticles (DOX-BNNPs) consisted of numerous nanosheet-like petals were tested on cell lines that differ in the multidrug resistance (MDR), namely two lines of human cervical carcinoma (KB-3-1 and MDR KB-8-5) and two lines of human chronic leukemia

(K562 and MDR i-S9). The maximum load capacity of BNNPs with DOX (180-200 μg/mg) was achieved after saturation in alkaline solution at pH 8.4. The DOX-BNNP nanoconjugates were internalized by both sensitive and MDR neoplastic cells and were well seen in cell cytoplasm between actin bundles, hereby showing perinuclear enrichment. Our study demonstrated a higher sensitivity of the leukemia lines to DOX-BNNPs compared with the carcinoma lines: IC_{50}(DOX-BNNPs) was 1.13, 4.68, 0.025, and 0.14 μg/ml for the KB-3-1, MDR KB-8-5, K562, and MDR i-S9 cell lines, respectively. Our estimates showed that it requires 1.2-7.5 (K562 cells) and 5.0-35 (IS9 cells) times less DOX conjugated with BNNPs to achieve IC_{50} compared with free DOX. In case of the DOX-BNNP nanoconjugates, the DOX penetration by endocytic mechanism was different from that of free DOX and allowed for maintaining a high and stable level of DOX in the nuclei of MDR KB-8-5 cells. This is a promising result for further development of drug-loaded nanocarriers based on nano-BN for the treatment of tumor diseases, in particular leukemia.

AUTHOR INFORMATION

Corresponding Authors

*E-mail: irazhitnyak@gmail.com

* E-mail: shtansky@shs.misis.ru

Notes

The authors declare no competing financial interest.

ACKNOWLEDGEMENTS

The work was supported by the Ministry of Education and Science of the Russian Federation (Increase Competitiveness Program of NUST “MISiS” No. K2-2016-011) and Russian Foundation for Basic Research (16-08-00957). We are grateful to Anastasiia Kalinina (Laboratory of regulatory mechanisms in immunity at N.N. Blokhin Cancer Research Center) for the help and advices in working on the flow cytometer. D.G. is grateful to the Australian Research Council for granting a Laureate Fellowship.

REFERENCES

(1) Knop, K.; Hoogenboom, R.; Fischer, D.; Schubert, U.S. Poly(ethylene glycol) in Drug Delivery: Pros and Cons as well as Potential Alternatives. *Angew. Chem. Int. Ed.* **2010**, *49*, 6288–6308.

(2) Torchilin, V.P.; Lukyanov, A.N. Peptide and Protein Drug Delivery to and into Tumors: Challenges and Solutions. *Drug Discov. Today.* **2003**, *8*, 259–266.

(3) Oerlemans, C.; Bult, W.; Bos, M.; Storm, G.; Nijsen, J.F.W.; Hennink, W.E. Polymeric Micelles in Anticancer Therapy: Targeting, Imaging and Triggered Release. *Pharm. Res.* **2010**, *27*, 2569–2589.

(4) Kaasgaard, T.; Andresen, T.L. Liposomal Cancer Therapy: Exploiting Tumor Characteristics. *Expert Opin. Drug Deliv*. **2010**, *7*, 225–243.

(5) Mintzer, M.A.; Grinstaff M.W. Biomedical Applications of Dendrimers: A Tutorial. *Chem. Soc. Rev*. **2011**, *40*, 173–190.

(6) Dreaden, E.C.; Mackey, M.A.; Huang, X.; Kang, B.; El-Sayed, M.A. Beating Cancer in Multiple Ways Using Nanogold. *Chem. Soc. Rev*. **2011**, *40*, 3391–3404.

(7) Lal, S.; Clare, S.E.; Halas, N.J. Nanoshell-Enabled Photothermal Cancer Therapy: Impending Clinical Impact. *Acc. Chem. Res*. **2008**, *41*, 1842–1851.

(8) Jokerst, J.V.; Gambhir, S.S. Molecular Imaging with Theranostic Nanoparticles. *Acc. Chem. Res.* **2011**. *44*, 1050–1060.

(9) Trewyn, B.G.; Slowing, I.I.; Giri, S.; Chen, H.-T.; Lin, V.S.Y. Synthesis and Functionalization of a Mesoporous Silica Nanoparticle Based on the Sol–gel Process and Applications in Controlled Release. *Acc. Chem. Res.* **2007**, *40*, 846–853.

(10) Bonacchi, S.; Genovese, D.; Juris, R.; Montalti, M.; Prodi, L.; Rampazzo, E.; Zaccheroni N. Luminescent Silica Nanoparticles. Extending the Frontiers of Brightness. *Angew. Chem. Int. Ed.* **2011**, *50*, 4056–4066.

(11) Xie, J.; Huang, J.; Li, X.; Sun, S.; Chen, X. Iron Oxide Nanoparticle Platform for Biomedical Applications. *Curr. Med. Chem.* **2009**, *16*, 1278–1294.

(12) Gottesman, M.M.; Fojo, T.; Bates, S.E. Multidrug Resistance in Cancer: Role of ATP-Dependent Transporters. *Nature Rev.* **2002**, *2*, 48–58.

(13) Amin L. P-glycoprotein Inhibition for Optimal Drug Delivery. *Drug Target Insights* **2013**, *7*, 27–34.

(14) Swan, S.M.; Whaley, F.S.; Ewer, M.S. Congestive Heart Failure in Patients Treated with Doxorubicin, *Cancer* **2003**, *97*, 2869-2879

(15) Thorn, C.F.; Oshiro, C.; Marsh, S.; Hernandez-Boussard, T.; McLeod, H.; Klein, T.E.; Altman, R.B. Doxorubicin Pathways: Pharmacodynamics and Adverse Effects. *Pharmacogenet Genomics* **2011**, *21*, 440–446.

(16) Kumari, P.; Ghosh, B.; Biswas, S. Nanocarriers for Cancer-Targeted Drug Delivery. *J Drug Target.* **2016**, *24*, 179-191.

(17) Gharpure, K.M.; Wu, S.Y.; Li, C.; Lopez-Berestein, G.; Sood, A.K. Nanotechnology: Future of Oncotherapy. *Clin. Cancer Res.* **2015**, *21*, 3121-3130.

(18) Liong, M.; Lu, J.; Kovochich, M.; Xia, T.; Ruehm, S.G..; Nel, A.E.; Tamanoi, F.; Zink J.I. Multifunctional Inorganic Nanoparticles for Imaging, Targeting, and Drug Delivery. *ACS Nano* **2008**, *2(5)*, 889–896.

(19) Elzoghby, A.O.; Hemasa, A.L.; Freag, M.S. Hybrid Protein-Inorganic Nanoparticles: From Tumor-Targeted Drug Delivery to Cancer Imaging, *J. Control. Release* **2016**, *243*, 303-322.

(20) Chen, X.; Sun, H.; Hu, J.; Ha, X.; Liu, H.; Hu, Y. Transferrin Gated Mesoporous Silica Nanoparticles for Redox-Responsive and Targeted Drug Delivery. *Colloids Surf. B: Biointerfaces* **2017**, *152*, 77-84.

(21) Gu, J.; Al-Bayati, K.; Ho, E.A. Development of Antibody-Modified Chitosan Nanoparticles for the Targeted Delivery of siRNA Across the Blood-Brain Barrier as a Strategy for Inhibiting HIV Replication in Astrocytes. *Drug Deliv. Transl. Res*. **2017**, *7(4)*, 497-506.

(22) Hu, C.M.; Zhang. L. Therapeutic Nanoparticles to Combat Cancer Drug Resistance. *Curr. Drug Metab.* **2009**, *10*, 836–841.

(23) Hu, C.M.; Zhang, L. Nanoparticle Based Combination Therapy Toward Overcoming Drug Resistance in Cancer. *Biochem Pharmacol.* **2012**, *83*, 1104–1111.

(24) Tacar, O.; Sriamornsak, P.; Dass, C.R. Doxorubicin: an Update on Anticancer Molecular Action, Toxicity and Novel Drug Delivery Systems. *J. Pharm. Pharmacol.* **2013,** *65*, 157-170.

(25) Barenholz, Y. Doxil – The First FDA-Approved Nano-Drug: Lessons Learned, *J. Controlled Release* **2012**, *160*, 117-134.

(26) Lyass, O.; Uziely, B.; Ben-Yosef, R.; Tzemach,D.; Heshing, N.I.; Lotem, M.; Brufman, G.; Gabizon, A. Correlation of Toxicity with Pharmacokinetics of Pegylated Liposomal Doxorubicin (Doxil) in Metastatic Breast Carcinoma. *Cancer* **2000**, *89(5)*, 1037-1047.

(27) Barenholz, Y. Doxil® — The First FDA-Approved Nano-Drug: Lessons Learned. *J. Control. Release* **2012**, *160*, 117–134.

(28) O'Brien, M. E. R. ; Wigler, N.; Inbar, M.; Rosso, R.; Grischke, E.; Santoro, A.; Catane, R.; Kieback, D.G.; Tomczak, P.; Ackland, S. P.; Orlandi, F.; Mellars, L.; Alland, L.; Tendler, C. Reduced Cardiotoxicity and Comparable Efficacy in a Phase III Trial of Pegylated Liposomal Doxorubicin HCl (CAELYX™/Doxil®) Versus Conventional Doxorubicin for First-Line Treatment of Metastatic Breast Cancer. *Ann. Oncol.* **2004**, *15(3)*, 440-449.

(29) Castillo, R.R.; Colilla, M.; Vallet-Regí, M. Advances in Mesoporous Silica-Based Nanocarriers for Co-Delivery and Combination Therapy Against Cancer. *Expert Opin. Drug Delivery* **2017***, 14*, 229-243.

(30) Ruibin, L.; Ren'an, W.; Liang, Z.; Minghuo, W.; Ling, Y.; Hanfa, Z. P-Glycoprotein Antibody Functionalized Carbon Nanotube Overcomes the Multidrug Resistance of Human Leukemia Cells, *ACS Nano* **2010**, *4*, 1399–1408.

(31) Ciofani, G.; Raffa, V.; Menciassi, A.; Cuschieri, A. Boron Nitride Nanotubes: An Innovative Tool for Nanomedicine. *Nano Today* **2009**, *4(1)*, 8-10.

(32) Şen, Ö.; Çobandede, Z; Emanet, M.; Bayrak, O.F.; Çulha, M. Boron Nitride Nanotubes for Gene Silencing. *Biochim. Biophys. Acta* **2017**, doi: 10.1016/j.bbagen.2017.05.026.

(33) Gao, C.; Feng, P.; Peng, S.; Shuai, C. Carbon Nanotube, Graphene and Boron Nitride Nanotube Reinforced Bioactive Ceramics for Bone Repair. *Acta Biomater.* **2017**, doi: 10.1016/j.actbio.2017.05.020.

(34) Graziana G.G.; Sinibaldi. E.; Ceseracciu, L.; Labardi, M.; Marino, A.; Marras. S.; De Simoni, G.; Mattoli, V.; Ciofani, C. Ultrasound-Activated Piezoelectric P(VDF-TrFE)/Boron Nitride Nanotube Composite Films Promote Differentiation of Human SaOS-2 Osteoblast-Like Cells. *Nanomedicine* **2017**, doi: 10.1016/j.nano.2017.05.006

(35) Li, X.; Zhi, C.; Hanagata, N.; Yamaguchi, M.; Bando, Y.; Golberg, D. Boron Nitride Nanotubes Functionalized with Mesoporous Silica for Intracellular Delivery of Chemotherapy Drug. *Chem. Comm.* **2013**, *49*, 7337-7339.

(36) Sukhorukova, I.V.; Zhitnyak, I.Y.; Kovalskii, A.M.; Matveev, A.T.; Lebedev, O.I.; Li, X.; Gloushankova, N.A.; Golberg, D.; Shtansky, D.V. Boron Nitride Nanoparticles with Petal-Like Surface as Anticancer Drug Delivery System. *ACS Appl. Mater. Interf.* **2015**, *7*, 17217-25.

(37) Li, X.; Wang, X.; Zhang, J.; Hanagata, N.; Wang, X.; Weng, Q.; Ito, A.; Bando, Y.; Golberg, D. Hollow Boron Nitride Nanospheres as Boron Reservoir for Prostate Cancer Treatment. *Nat. Commun.* **2017**, *8*, 13936.

(38) Kovalskii, A.M.; Matveev, A.T.; Lebedev, O.I.; Sukhorukova, I.V.; Firestein, K.L.; Steinman, A.E.; Shtansky, D.V.; Golberg, D. Growth of Spherical Boron Oxynitride Nanoparticles with Smooth and Petalled Surfaces During Chemical Vapor Deposition Process, *CrystEngComm.* **2016**, *18*, 6689-6699.

(39) Akiyama, S.; Fojo, A.; Hanover, J.A.; Pastan, I.; Gottesman, M.M. Isolation and Genetic Characterization of Human KB Cell Lines Resistant to Multiple Drugs. *Somat. Cell Molec. Gen*. **1985**, *11*, 117-126.

(40) Richert, N.; Akiyama, S.; Shen, D.-W.; Gottesman, M.M.; Pastan, I. Multiply Drug-resistant Human KB Carcinoma Cells Have Decreased Amounts of a 75-kDa and a 72-kDa Glycoprotein. *Proc. Natl. Acad. Sci. USA* **1985**, *82*, 2330-2333.

(41) Park, S.W.; Lomri, N.; Simeoni, L.A.; Fruehauf, J.P.; Mechetner, E. Analysis of P-Glycoprotein–Mediated Membrane Transport in Human Peripheral Blood Lymphocytes Using the UIC2 Shift Assay. *Cytometry* **2003**, *53A*, 67–78.

(42) Das, G.; Nicastri, A.; Coluccio, M. L.; Gentile, F.; Candeloro, P.; Cojoc, G.; Liberale, C.; De Angelis, F.; Di Fabrizio, E. FT-IR, Raman, RRS Measurements and DFT Calculation for Doxorubicin, *Microsc. Res. Techniq.* **2010**, *73*, 991–995.

(43) Rudra, A.; Deepa, R.M.; Ghosh, M.K.; Ghosh, S.; Mukherjee, B. Doxorubicin-loaded Phosphatidylethanolamine-Conjugated Nanoliposomes: in Vitro Characterization and Their Accumulation in Liver, Kidneys, and Lungs in Rats. *Int. J Nanomed.* **2010**, *5*, 811–823.

(44) Li, J.M.; Zhang, W.; Su, H.; Wang, Y.Y.; Tan, C.P.; Ji, L.N.; Mao, Z.W. Reversal of Multidrug Resistance in MCF-7/Adr Cells by Codelivery of Doxorubicin and BCL2 siRNA Using a Folic Acid-conjugated Polyethylenimine Hydroxypropyl-β-cyclodextrin Nanocarrier. *Int. J. Nanomed.* **2015**, *10*, 3147–3162.

(45) Wörle-Knirsch, J.M.; Pulskamp, K.; Krug, H.F. Oops They Did It Again! Carbon Nanotubes Hoax Scientists in Viability Assays. *Nano Lett.* **2006**, *6*, 1261-1268.

(46) Ciofani, G.; Danti, S.; D'Alessandro, D.; Moscato, S.; Menciassi, A. Assessing Cytotoxicity of Boron Nitride Nanotubes: Interference with the MTT Assay. *Biochem. Biophys. Res. Commun.* **2010**, *394(2)*, 405-411.

(47) Termsarasab, U.; Yoon, I.S.; Park, J. H.; Moon, H.T.; Cho, H.J.; Kim, D.D. Polyethylene Glycol-Modified Arachidyl Chitosan-Based Nanoparticles for Prolonged Blood Circulation of Doxorubicin. *Int. J. Pharm.* **2014**, *464*, 127-134.

(48) Chithrani, B.D.; Chan, W.C. Elucidating the Mechanism of Cellular Uptake and Removal of Protein-Coated Gold Nanoparticles of Different Sizes and Shapes. *Nano Lett.* **2007**, *7*, 1542-1550.

(49) Huang, X.; Teng, X., Chen, D.; Tang, F.; He, J. The Effect of the Shape of Mesoporous Silica Nanoparticles on Cellular Uptake and Cell Function. *Biomaterials* **2010**, *31*, 438–448.

(50) Barraud, L.; Merle, P.; Soma, E.; Lefrançois, L. ; Guerret, S. ; Chevallier, M. ; Dubernet, C. ; Couvreur, P. ; Trépo, C. ; Vitvitski, L. Increase of Doxorubicin Sensitivity by Doxorubicin-Loading into Nanoparticles for Hepatocellular Carcinoma Cells in Vitro and in Vivo, *J. Hepatol.* **2005**, *42*, 736–743.

(51) Weng, K.C.; Noble, C.O.; Papahadjopoulos-Sternberg, B.; Chen, F.F.; Drummond, D.C.; Kirpotin, D.B.; Wang, D.; Hom, Y.K.; Hann, B.; Park, J.W. Targeted Tumor Cell Internalization and Imaging of Multifunctional Quantum Dot-Conjugated Immunoliposomes in Vitro and in Vivo, *Nano Lett.* **2008**, *8*, 2851–2857.

(52) Chen, A.M.; Zhang, M.; Wei, D.; Stueber, D.; Taratula, O.; Minko, T.; He, H. Co-delivery of Doxorubicin and Bcl-2 siRNA by Mesoporous Silica Nanoparticles Enhances the Efficacy of Chemotherapy in Multidrug-Resistant Cancer Cells. *Small* **2009**, *5*, 2673–2677.

(53) Xia, H.; Mao, Q.; Paulson, H.L.; Davidson, B.L. siRNA-mediated Gene Silencing in Vitro and in Vivo. *Nature Biotechn.* **2002**, *20*, 1006 - 1010.

(54) Fedorov, Y.; Anderson, E.M.; Birmingham, A.; Reynolds, A.; Karpilow, J.; Robinson, K.; Leake, D.; Marshall, W.S.; Khvorova, A. Off-target Effects by siRNA Can Induce Toxic Phenotype. *RNA* **2006**, *12*, 1188-1196.

(55) Shuhendler, A.J.; Cheung, R.Y.; Manias, J.; Connor, A.; Rauth, A.M.; Wu, X.Y. A Novel Doxorubicin-Mitomycin C Co-Encapsulated Nanoparticle Formulation Exhibits Anti-Cancer Synergy in Multidrug Resistant Human Breast Cancer Cells. *Breast Cancer Res. Treat.* **2010**, *119*, 255–269.

(56) Qiu, L.Y., Wang, R.J., Zheng, C.; Jin, Y.; Jin. L.Q. Beta-Cyclodextrin-Centered Star-shaped Amphiphilic Polymers for Doxorubicin Delivery. *Nanomed.* **2010**, *5*, 193–208.

(57) Ciofani, G.; Danti, S.; Genchi, G.G., D'Alessandro, D.; Pellequer, J.L.; Odorico, M.; Mattoli, V.; Giorgi, M. Pilot in Vivo Toxicological Investigation of Boron Nitride Nanotubes, *Int. J. Nanomed.* **2012**, *7*, 19-24.

(58) Ciofani, G.; Danti, S.; Nitti, S.; Mazzolai, B.; Mattoli, V.; Giorgi, M. Biocompatibility of Boron Nitride Nanotubes: An Up-Date of in Vivo Toxicological Investigation. *Int. J. Pharmaceutics* **2013**, *444*, 85-88.

(59) Emanet, M.; Şen, Ö.; Çulha, M. Evaluation of Boron Nitride Nanotubes and Hexagonal Boron Nitrides as Nanocarriers for Cancer Drugs. *Nanomedicine* **2017**, *12(7)*, 797-810.

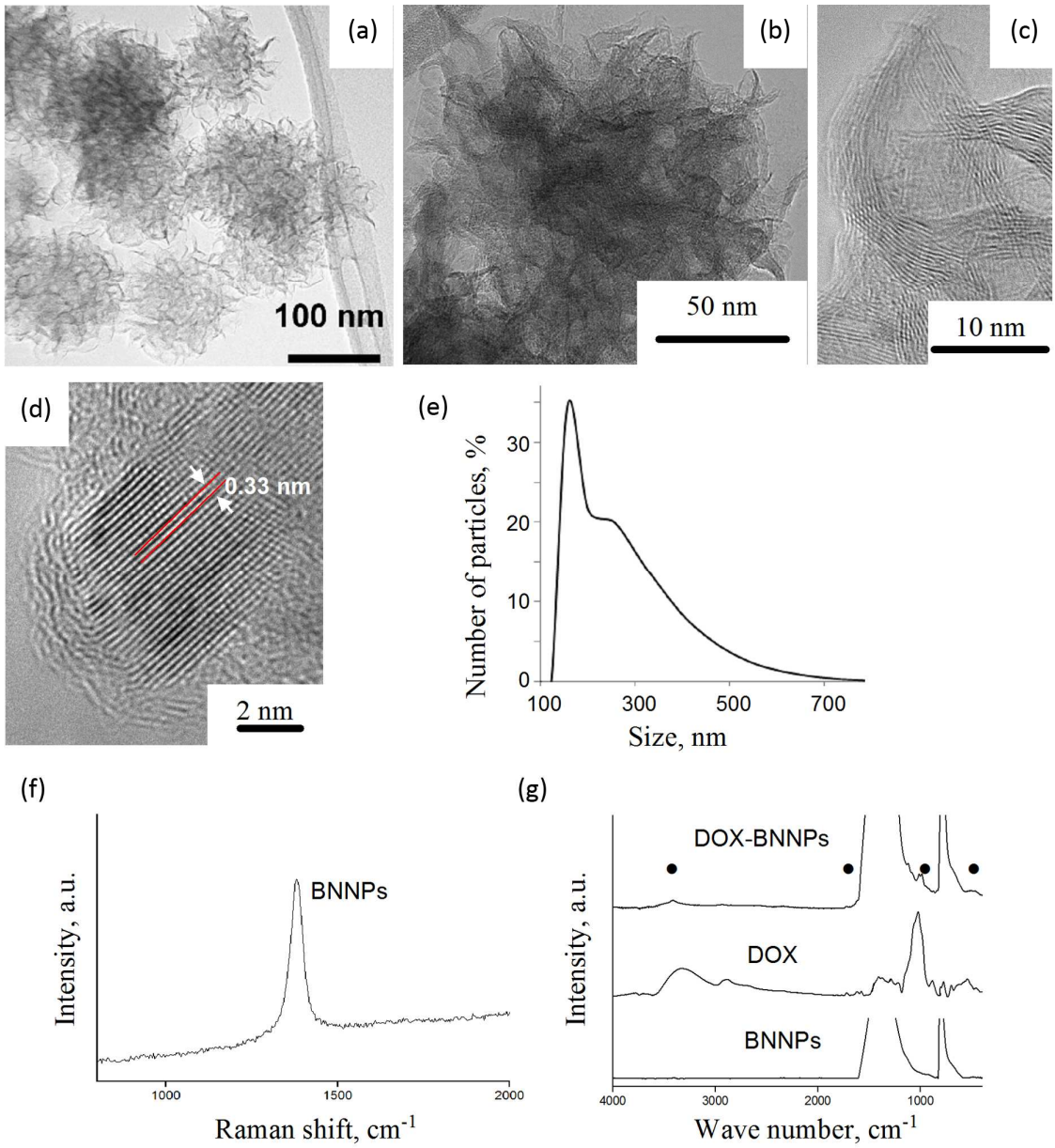

Figure 1. TEM images of (a, b) BNNPs and (c, d) their nanosheet-like petals, (e) BNNP size distribution after ultrasonic treatment, (f) Raman spectrum of BNNPs, and (g) FTIR spectra of DOX, BNNPs, and DOX-BNNPs. (•) DOX peaks observed on the DOX-BNNP spectrum.

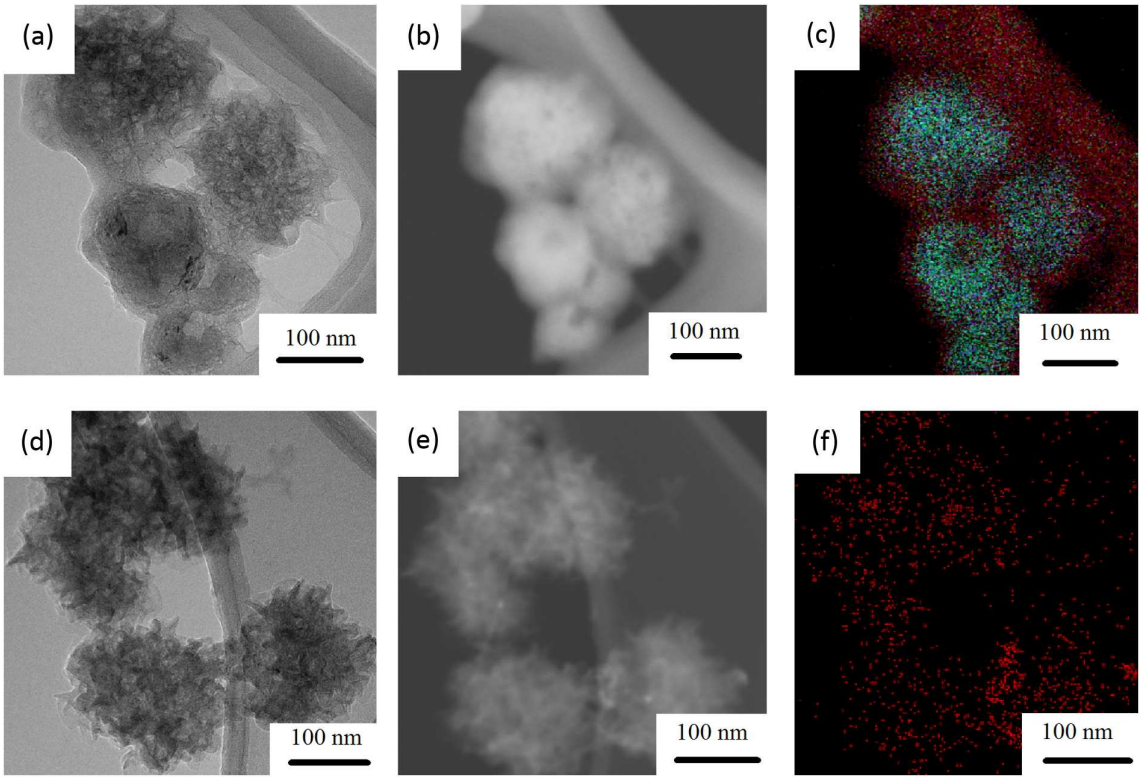

Figure 2. BNNPs loaded with (a-c) doxorubicin and (d-f) carboplatin. (a, d) Bright field TEM images, (b, e) HADF - STEM images, and (c, f) corresponding spatially-resolved EDX maps showing (c) carbon and (f) platinum distribution.

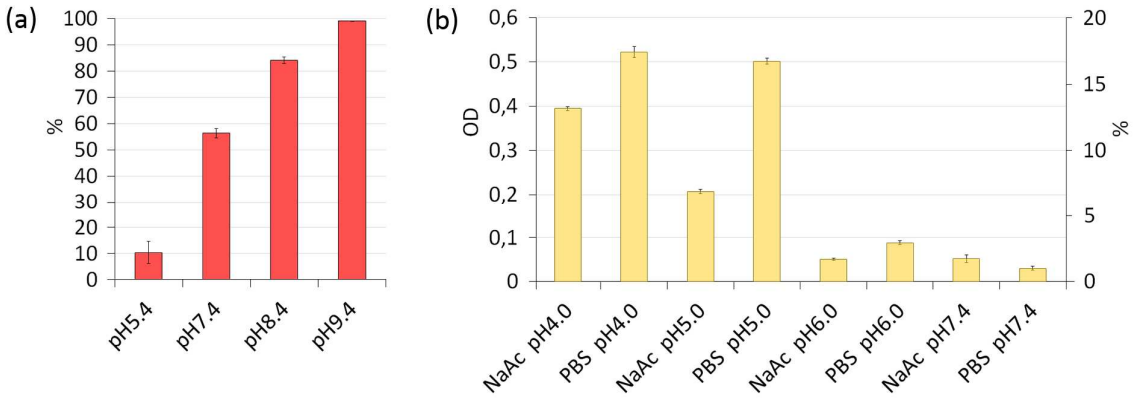

Figure 3. (a) Efficiency of DOX loading into BNNPs at various pH of sodium acetate buffer DOX solutions. DOX-BNNPs saturated in alkaline solutions revealed higher DOX loading than DOX-BNNPs saturated in neutral or acid media. Data are presented as a percentage of the DOX content in DOX-BNNPs to amount of DOX in DOX solution used for saturation. (b) pH-dependent DOX release from DOX-BNNPs for 24 h. Left Y-axis – OD of supernatant. Right Y-axis – the percentage of released DOX (the amount of released DOX to the DOX content in DOX-BNNPs).

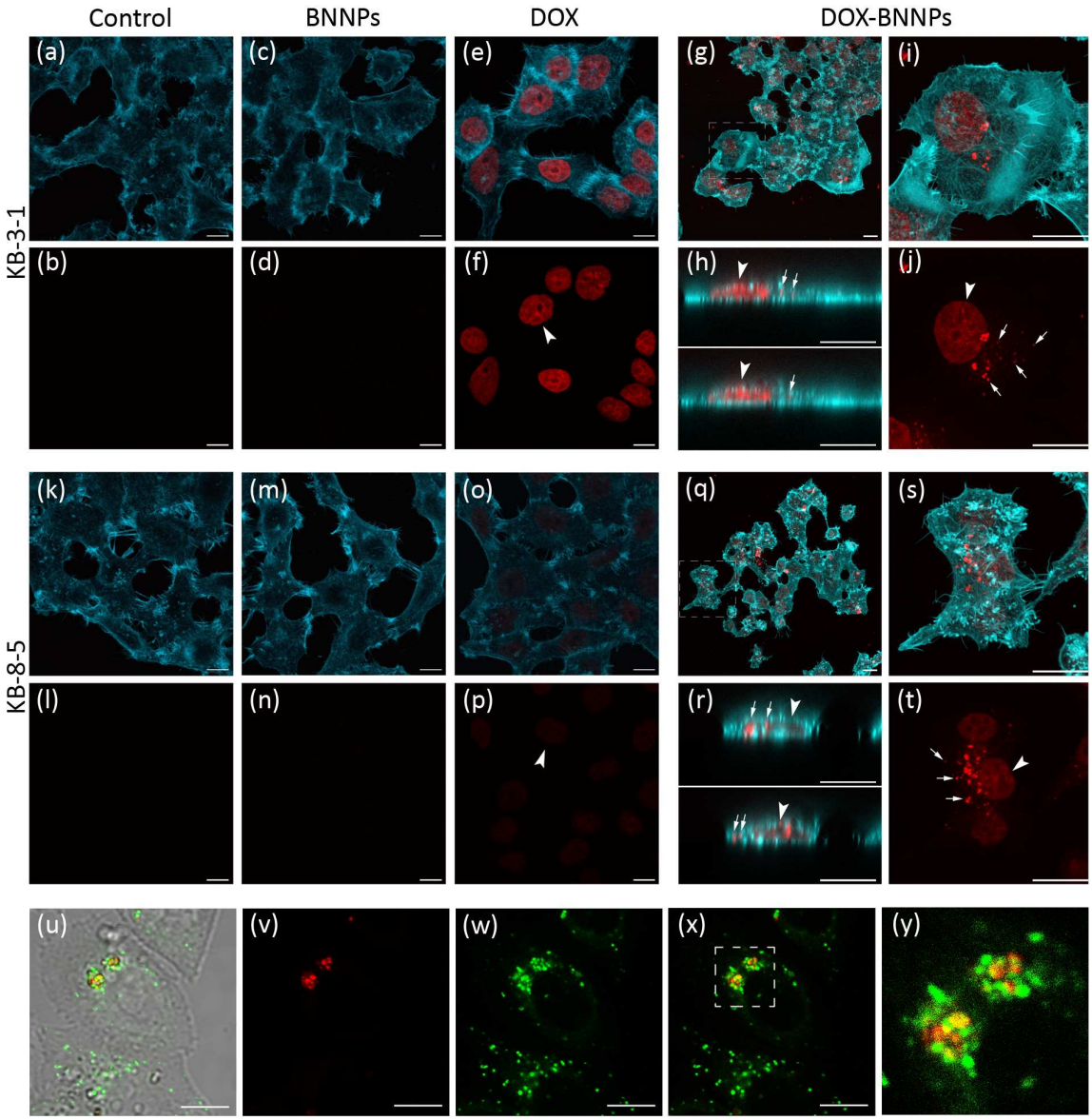

Figure 4. CLSM images of KB-3-1 (a-j) and KB-8-5 (k-t) cells treated with BNNPs, free DOX, and DOX-BNNPs in comparison with the control. (a-s) Alexa488-phaloidin staining of actin cytoskeleton (cyan) and fluorescence of DOX (red). (a-f and k-p) 4 h of incubation. (g-i and q-t) Cells incubated with DOX-BNNPs for 24 h. (i and s) Close-up views of the boxed region from g and q, respectively. (h and r) XZY slides of the cell. DOX-BNNPs are seen near the nucleus (arrows). Red fluorescence of DOX in the nucleus is shown by arrowheads. (u-y) Confocal images (differential interference contrast and fluorescent channels) of KB-8-5 cells. Cells were incubated with DOX-BNNPs for 8 h and were stained with LysoTracker Green. (x) DOX-BNNPs (red) are colocalized with lysosomes. (y) A close-up view of the boxed region from (x). Scale bar 10 μm.

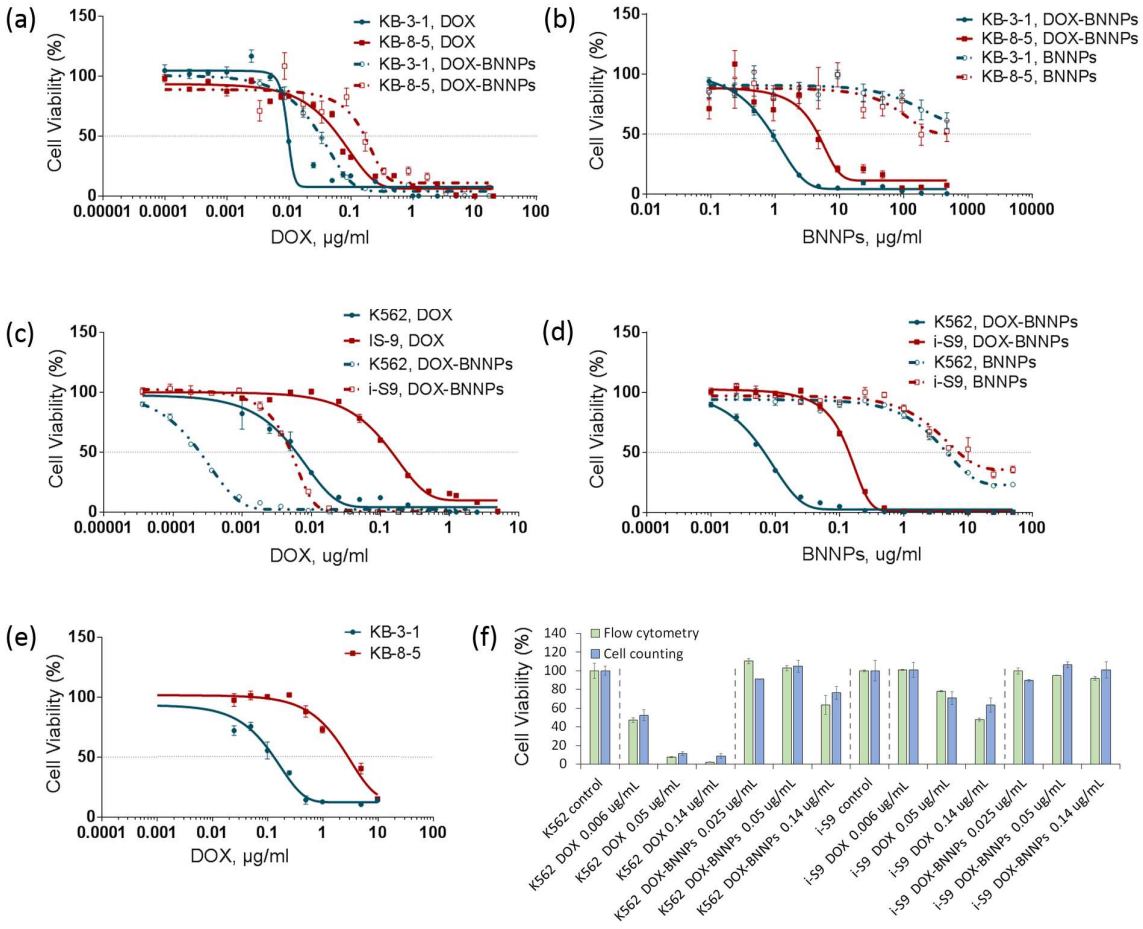

Figure 5. (a-d) Effect of DOX, pristine BNNPs, and DOX-BNNP conjugates on the viability of (a, b) KB-3-1 and KB-8-5 cells, and (c, d) K562 and i-S9 cells. (a, b) Cell counting tests. (c, d) Flow cytometry. Sigmoidal non-linear regression, the concentration is shown as log10, a dotted line marks a 50% viability level. (e) MTT test for free DOX. (f) Comparison of flow cytometric test and cell counting test. K562 and i-S9 were treated with DOX or DOX-BNNPs for 72 h.

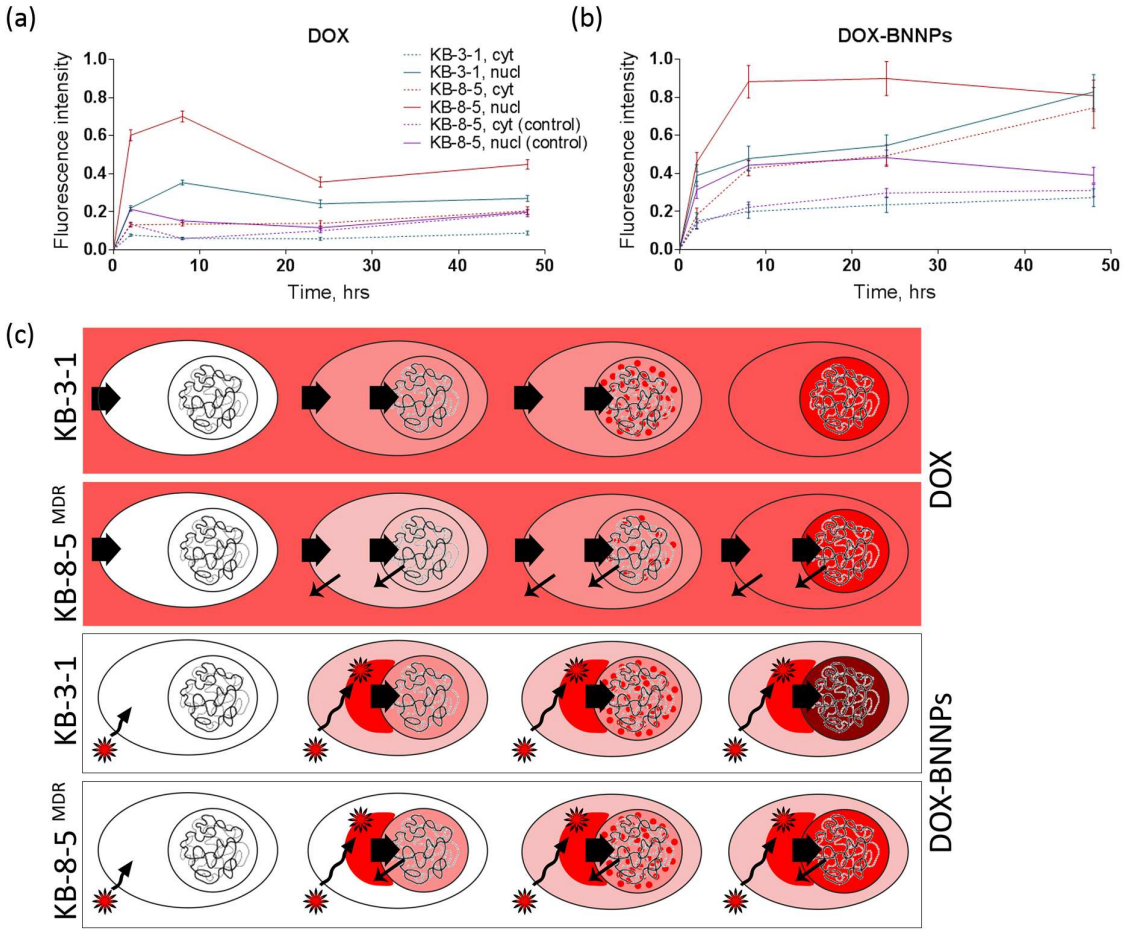

Figure 6. Fluorescence intensity of DOX in nucleus and cytoplasm of KB-3-1 and KB-8-5 cells treated with DOX (a) and DOX-BNNPs (b). IC_{50} concentrations of free DOX and DOX-BNNP solutions for each cell type were obtained from cell counting assay (Fig. 3). For KB-8-5 cells IC_{50} determined for KB-3-1 cells was also used (designated as KB-8-5 (control)). (c) Hypothetical schema of DOX redistribution in cells treated with free DOX and DOX-BNNPs. Free DOX entries through the cell membrane into the cytoplasm and then penetrates into the nucleus via diffusion (wide arrow) binding with DNA. In MDR KB-8-5 cells, activation of MDR mechanisms is shown (thin arrow). DOX-BNNPs penetrate into the cells via endocytosis (waved arrow). The influx of DOX into the nucleus from perinuclear zone *via* diffusion is shown with wide arrow.

Table 1. IC_{50}(DOX) and IC_{50}(DOX-BNNPs) for Different Cell Lines

cell line	IC_{50}(DOX), μg/ml	IC_{50}(DOX-BNNPs), μg/ml		
		BNNPs	loaded DOX	released DOX within 24 h
KB-3-1	0.011	1.130	0.224	0.035
KB-8-5	0.061	4.680	0.927	0.143
K562	0.006	0.025	0.005	0.0008
i-S9	0.140	0.140	0.028	0.004

Graphical abstract